Received 14 December 2023; revised 28 February 2024; accepted 1 March 2024. Date of publication 18 March 2024; date of current version 21 March 2024.
The review of this article was arranged by Editor M. Wong.

Digital Object Identifier 10.1109/JEDS.2024.3373905

Fermi-Level Splitting-Induced Light-Intensity-Dependent Recombination in Fully Ultra-Wide Bandgap Deep-Ultraviolet Photodetector

WANYU MA[1,2,3], MAOLIN ZHANG[1,2,3] (Member, IEEE), LEI WANG[1,2,3], SHAN LI[1,2,3] (Member, IEEE), LILI YANG[1,2,3], ZENG LIU[1,2,3] (Member, IEEE), YUFENG GUO[1,2,3] (Member, IEEE), AND WEIHUA TANG[1,2,3] (Member, IEEE)

1 College of Integrated Circuit Science and Engineering, Nanjing University of Posts and Telecommunications, Nanjing 210023, China
2 Innovation Center for Gallium Oxide Semiconductor, Nanjing University of Posts and Telecommunications, Nanjing 210023, China
3 National and Local Joint Engineering Laboratory for RF Integration and Micro-Assembly Technologies, Nanjing University of Posts and Telecommunications, Nanjing 210023, China

CORRESPONDING AUTHORS: M. ZHANG, Y. GUO, and W. TANG (e-mail: mlzhang@njupt.edu.cn; yfguo@njupt.edu.cn; whtang@njupt.edu.cn)

This work was supported in part by the National Key Research and Development Program of China under Grant 2022YFB3605404; in part by the China Post-Doctoral Science Foundation under Grant 2022M721689; in part by the Jiangsu Funding Program for Excellent Post-Doctoral Talent; and in part by the National Natural Science Foundation of China under Grant 62304113 and Grant 62204125.

ABSTRACT Ga_2O_3-based heterojunction features the capability of self-driven detection, which is reckoned as a promising candidate for the next-generation deep-ultraviolet (DUV) sensing scenarios. Heterojunction consisting of fully ultra-wide bandgap (UWB) semiconductors would prevent additional response in the near-ultraviolet band. In this work, a β-Ga_2O_3/AlN heterojunction photodetector is constructed and its operating mechanisms are investigated. By measuring its static current-voltage (I-V) and dynamic current-time (I-t) characteristics, the detection performance, including a photo-to-dark current ratio of 8.6×10^5, a responsivity of 0.41 mA/W, a specific detectivity of 3.4×10^{12} Jones, and an external quantum efficiency of 0.2% were achieved under 0 V bias, indicating that the proposed device realized high-performance self-driven detection. Moreover, this work demonstrated the impact of Fermi-level splitting introduced by the enhanced photo illumination on the carrier recombination and the sensing performance. With the increase of light intensity, Fermi levels are separated and available recombination centers are increased, leading to the enhancement of the recombination process and the variation of detection properties. Consequently, this work highlights the potential of the fully UWB heterojunction and provides further optimization guidelines.

INDEX TERMS β-Ga_2O_3, AlN, heterojunction, photodetector, deep-ultraviolet, recombination.

I. INTRODUCTION

Deep-ultraviolet (DUV) photodetection is less subject to interference from the sunlight since solar irradiation of wavelength shorter than 280 nm rarely reaches the earth's ground. This leads to the important applications of DUV detection in a variety of fields, including scientific research and civilian as well as military equipment [1], [2], [3], [4], [5], [6], [7]. Ultra-wide bandgap semiconductor Ga_2O_3 presents a unique advantage in the DUV sensing application because of its large bandgap of >4.6 eV. Recently, various Ga_2O_3-based photodetectors including metal-semiconductor-metal (MSM), Schottky barrier diodes (SBDs), field-effect transistors (FETs), and heterojunctions have been proposed and demonstrated with promising detecting efficiency [8], [9], [10], [11], [12], [13], [14], [15], [16].

Ga_2O_3-based heterojunction photodetectors usually composite two materials to form the band alignment and the built-in potential, thereby photo-generated carriers can be driven even without a bias voltage. In addition, the built-in potential prevents carrier transport in the dark

© 2024 The Authors. This work is licensed under a Creative Commons Attribution-NonCommercial-NoDerivatives 4.0 License.
For more information, see https://creativecommons.org/licenses/by-nc-nd/4.0/

condition and a low dark current can be also achieved. Hence, heterojunction is favored in low-power consumption scenarios. Various semiconductors have been integrated with Ga_2O_3 to construct a heterojunction DUV sensor including ZnO/Ga_2O_3 [17], SnO_2/Ga_2O_3 [18], GaN/Ga_2O_3 [19], and SiC/Ga_2O_3 [20]. These detectors show decent self-driven capability and low dark current thanks to the built-in barrier. However, most reported hetero-materials are of a lower bandgap semiconductor compared to Ga_2O_3. The advantage of ultra-wide bandgap (UWB) such as low response to the near-ultraviolet could be undermined. Therefore, a full UWB heterojunction may sustain the self-powered characteristics as well as the benefits of UWB semiconductors [21], [22].

Meanwhile, lattice mismatch is a crucial issue for heterojunctions as it is the main reason for the interfacial states. A significant number of surface states will act as the recombination centers and exhibit a non-negligible impact on the carrier transport as well as the recombination process. The most thermally stable polymorphs of Ga_2O_3, i.e., monoclinic β-Ga_2O_3 usually exhibit large mismatch to other semiconductors [23]. Therefore, a study of the sensor performance for a β-Ga_2O_3-based heterojunction through exploring the recombination process is critical.

In this work, a fully ultra-wide bandgap self-powered photodetector based on β-Ga_2O_3/AlN heterojunction was demonstrated. The nanofilms of β-Ga_2O_3/AlN were constructed by using the metalorganic chemical vapor deposition (MOCVD) and radio-frequency (RF) sputter technique. Its sensor performance including the static and the dynamic characteristics were measured. Besides, various detection-related figure-of-metrics (FOMs) were calculated and studied under different light intensities and biased voltages. Most importantly, the impact of the recombination centers on the photocurrent linearity, dynamic current surge, and response time was evaluated and discussed.

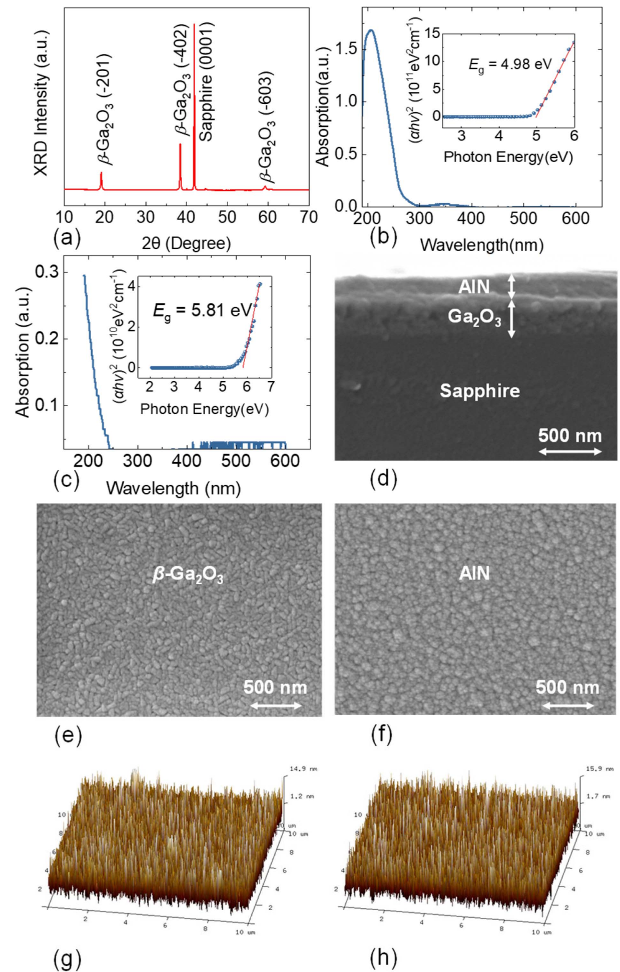

FIGURE 1. (a) XRD θ-2θ scan of the β-Ga_2O_3/AlN heterojunction. (b) UV–vis absorbance spectrum of the β-Ga_2O_3 film. (c) UV–vis absorbance spectrum of the AlN film. (d) SEM image of the cross-section for the β-Ga_2O_3/AlN heterojunction. (e) and (f) are the surface SEM images of the β-Ga_2O_3 and the AlN, respectively. (g) and (h) are the AFM images of the β-Ga_2O_3 and the AlN, respectively

II. EXPERIMENTAL

β-Ga_2O_3 nanofilms were prepared through MOCVD hetero-epitaxy on (0001) sapphire substrates. During epitaxy growth, the chamber temperature and the pressure were ∼750 °C and 25 Torr, respectively. Followed by the AlN film deposition using radio-frequency (RF) sputtering. The parameters of RF sputtering are as follows: the RF power was set to 175 W and the deposition time was 2 hours; the substrate temperature is 300 K and the chamber pressure is 0.75 Pa. No further annealing process was conducted. Note that no dopant was introduced during the film deposition. Therefore, high-resistance thin films would be formed. Subsequently, Ti/Au electrodes were formed by using the direct-current (DC) magnetron sputtering and a Cr-metal hard mask. The quality of the β-Ga_2O_3/AlN heterojunction was verified by X-ray diffraction (XRD), scanning electron microscope (SEM), UV-visible (UV-vis) absorbance spectrum, and atomic force microscopy (AFM). A 254 nm UV lamp was adopted as the DUV light source and the light intensity was adjusted by changing the distance from the light source to the measured sample. A semiconductor analyzer Agilent B1505A with a high-resolution source measurement unit (HR SMU, minimum measured current of 1 fA) was used to record the current-voltage (*I-V*) and current-time (*I-t*) curves of the heterojunction photodetector.

III. RESULTS AND DISCUSSION

In this section, we first characterize the crystal quality of the deposited β-Ga_2O_3/AlN films by XRD, SEM, UV-vis, and AFM measurements, as shown in Fig. 1. In Fig. 1(a), the $(\bar{2}01)$, $(\bar{4}02)$ and $(\bar{6}03)$ planes of the β-Ga_2O_3 can be observed. In addition, (0001) sapphire substrate was also verified from the XRD results. No visible peaks of the AlN are seen in Fig. 1(a), suggesting its low crystallinity. Fig. 1(b) shows the UV-vis absorbance spectrum of the β-Ga_2O_3 thin film. It is seen that the β-Ga_2O_3 has marginal absorbance in the visible range but exhibits a rather high absorption in the DUV band, indicating significant

photoresponse shall be presented under DUV radiation. Based on the Tauc relationship, the optical bandgap E_g of the deposited β-Ga_2O_3 can be obtained from the following equation:

$$(\alpha hv)^2 = C\left(hv - E_g\right) \tag{1}$$

where α is the absorption coefficient, C is a constant, and hv is the photon energy of the incident light. By extrapolating the $(\alpha hv)^2$ and hv, as seen in the inset figure of Fig. 1(b), the optical bandgap of β-Ga_2O_3 is calculated to be 4.98 eV. In Fig. 1(c), the optical bandgap of the AlN was also determined by the same approach. The cut-off wavelength for the AlN is shorter than the β-Ga_2O_3, which is less than 250 nm, and thus is expected to form a self-powered photodetection without introducing a response to the near-ultraviolet band. Consequently, the measured bandgap of AlN is 5.81 eV. Fig. 1(d) depicts the cross-sectional SEM image of the β-Ga_2O_3/AlN heterojunction. The thickness of the β-Ga_2O_3 and the AlN films are measured to be ~260 nm and ~180 nm, respectively. Fig. 1(e) and 1(f) display surface SEM images of the β-Ga_2O_3 and the AlN, with grain sizes of approximately 50 nm and 80 nm, respectively. Meanwhile, Fig. 1(g) and 1(h) present their AFM images, indicating roughness of 3.84 nm for β-Ga_2O_3 and 3.95 nm for AlN.

Fig. 2(a) is the device diagram of the fabricated β-Ga_2O_3/AlN heterojunction photodetector. Fig. 2(b) displays a top view of the device observed under a microscope. The effective illuminated area of the device is 2.25 mm^2. In Fig. 2(c), the *I-V* characteristics in the dark condition and under various light intensities are compared. With the successful fabrication of the high-resistance films and the formation of built-in potential, the minimum dark current was measured to be ~1 fA, which approaches the lowest measurable value. Under the 254 nm DUV illumination, the termination current is improved up to 10^{-8} A. At a 0 V bias voltage, a photocurrent of $>10^{-10}$ A was also measured, suggesting that the self-powered mode is achieved. An open circuit voltage of ~0.5 V is obtained due to the built-in potential. In addition, a greater photocurrent was obtained with a higher light intensity, and the linearity of the photocurrent will be discussed later. It can be calculated that the photo-to-dark current ratio *PDCR* of the detector under 0 V bias is near 10^6, which is superior to most reported Ga_2O_3 photodetectors [24], [25], [26].

In Fig. 2(d), the photocurrent as a function of the light intensity with various bias voltages is presented. According to a power law [27]: $I_{\text{photo}} \sim kP^{\theta}$, where I_{photo} is the photocurrent, k is a constant, and P is the light intensity. The linearity can be represented by the value of θ. The slope k of the fitting line is increased with a higher bias voltage due to the enhanced electric field. Meanwhile, $\theta<1$ was extracted for all bias voltages. Ideally, the θ should be unity providing that a stable carrier recombination process was established. In Rose's model [28], both situations where $\theta<1$ and $\theta>1$

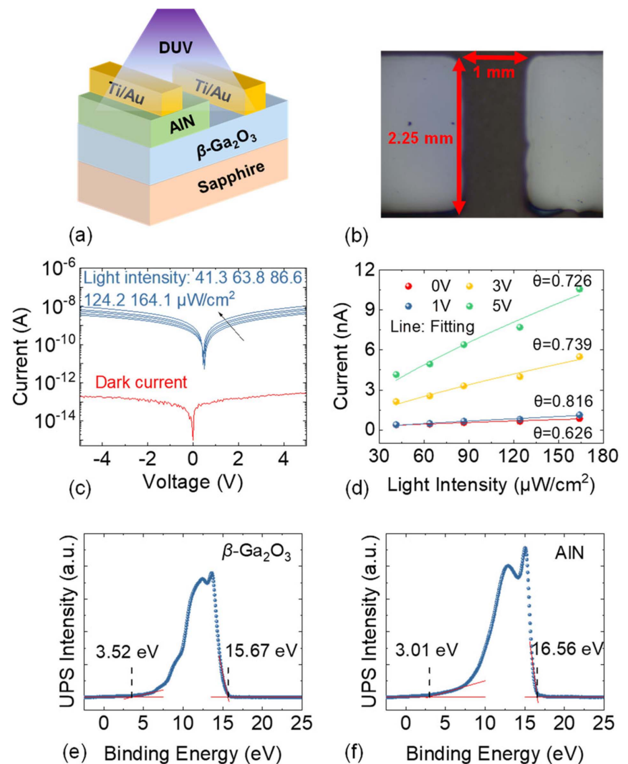

FIGURE 2. (a) Device diagram and (b) top-view micrograph of the β-Ga_2O_3/AlN heterojunction photodetector. (c) Dark current and photocurrent curves with various light intensities. (d) Light-intensity-dependent photocurrent of β-Ga_2O_3/AlN heterojunction. (e) and (f) are the ultraviolet photoelectron spectroscopy of the β-Ga_2O_3 and the AlN, respectively.

were thoroughly discussed and can be well applied in the sub-linearity phenomenon of this work.

Fig. 2(e) and 2(f) present the ultraviolet photoelectron spectroscopy (UPS) for β-Ga_2O_3 and AlN, respectively. The calculated work functions of β-Ga_2O_3 and AlN are 21.22-15.67=5.55 eV and 21.22-16.56=4.66 eV respectively, where 21.22 is the energy value of helium discharge lamp photons. Additionally, the valence band edge values (relative to the Fermi level) for both materials are extracted to be 3.52 eV and 3.01 eV, respectively.

To gain insight into the self-powered operational mechanism and sub-linear photocurrent behavior, Fig. 3(a) and 3(b) depict the energy band diagrams of the β-Ga_2O_3/AlN heterojunction before and under illumination. Based on the measured bandgaps and UPS data of the β-Ga_2O_3 and AlN, a valence band offset of 1.40 eV and a conduction band offset of 2.23 eV were obtained. The β-Ga_2O_3/AlN heterojunction exhibits a typical type II heterojunction. With a DUV illumination, photo-generated electrons are excited from the valence band to the conduction band. The carriers are then transported by the built-in electric field and the self-driven photocurrent is formed.

Due to the lattice mismatch between the AlN and the β-Ga_2O_3, the interface states as well as the bulk defects are expected to behave as the main recombination centers. These

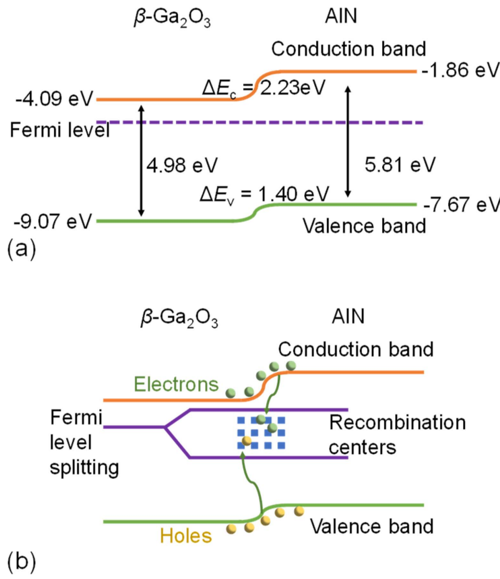

FIGURE 3. Energy band diagram of the β-Ga_2O_3/AlN heterojunction (a) before illumination and (b) under illumination.

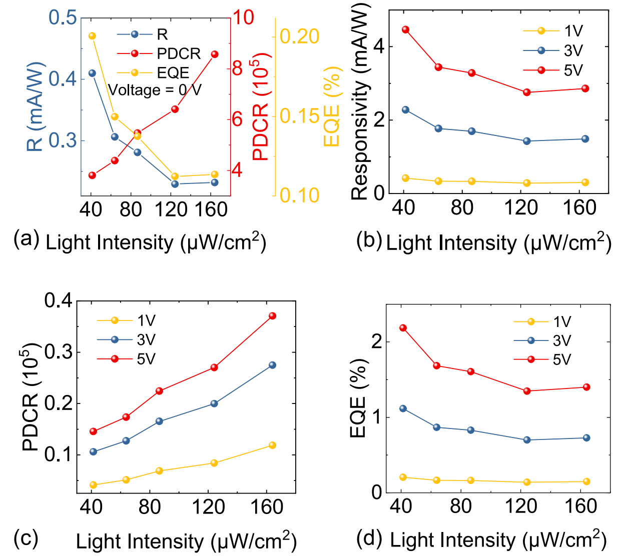

FIGURE 4. (a) Responsivity *R*, photo-to-dark current ratio *PDCR*, and external quantum efficiency *EQE* at 0 V bias. (b)-(d) are *R*, *PDCR*, and *EQE* at various applied voltages, respectively.

centers are critical for the carrier transport process. For a better understanding, Fig. 3(b) also illustrates the recombination centers. Without DUV illumination, a thermal equilibrium was achieved and the photodetector has a unified Fermi level. Under the DUV light illumination, carriers are generated and the quasi-Fermi-level for electrons (QFLE) and quasi-Fermi-level for holes (QFLH) are separated due to the nonequilibrium carriers' generation. With the enhancement of the light intensity, more carriers are generated and thus the quasi-Fermi-levels (QFLs) are more separated, leading to the increase of unoccupied recombination centers. Consequently, the recombination rate is improved and the concentration of available carriers that can form the photocurrent is reduced, resulting in the deviation of the intensity-photocurrent curve from linearity.

It is well known that the external voltage can also lead to the nonequilibrium carrier injection. In other words, as the biased voltage increases, QFLs would be separated as well and the θ should be further reduced. However, the θ exhibits no correlation with the applied voltage, which can be found in Fig. 2(d). This implies that the QFLs' separation is mainly determined by the incident DUV light rather than the applied voltage.

We then examine the detection figure-of-merits (FOMs) including responsivity R, photo-to-dark current ratio $PDCR$, detectivity D^*, and external quantum efficiency EQE, which are described in equation (2)–(5):

$$R = \frac{(I_{photo} - I_{dark})}{P \cdot S} \quad (2)$$

$$PDCR = \frac{I_{photo}}{I_{dark}} \quad (3)$$

$$D^* = \frac{R}{\sqrt{2q\frac{I_{dark}}{S}}} \quad (4)$$

$$EQE = \frac{Rhc}{q\lambda} \quad (5)$$

where I_{photo} and I_{dark} are the photocurrent and dark current, respectively, P is the light intensity, S is the effective illuminated area, q is the elementary charge, h is Planck's constant, c is the light velocity, and λ is the light wavelength. In Fig. 4(a), the R, $PRCR$, and the EQE of the β-Ga_2O_3/AlN sensor at 0 V bias are extracted. At a light intensity of 41.3 μW/cm^2, a maximum responsivity of 0.41 mA/W is obtained. In addition, a $PDCR$ of 8.6×10^5 and an EQE of 0.2% is achieved. The detectivity of 3.4×10^{12} Jones was obtained at a light intensity of 41.3 μW/cm^2. Meanwhile, all the FOMs are degraded at a higher light intensity. Photodetection FOMs fundamentally depend on the competition between carrier transport and recombination processes. In detail, higher transport efficiency leads to the improvement of FOMs mentioned above. The interface recombination states and bulk defect states in β-Ga_2O_3 and AlN can lead to the re-capture and recombination of photogenerated charge carriers, impeding their efficient transport to the electrodes. The improvement of interface and bulk quality is beneficial to the FOMs of a heterojunction photodetector [29], [30], [31], [32], [33]. Nevertheless, Table 1 provides a comparison of the self-powered performance between various Ga_2O_3 heterojunction photodetectors [34], [35], [36], [37], [38], [39]. The proposed β-Ga_2O_3/AlN heterojunction photodetector exhibits excellent detection capabilities.

The carrier transport efficiency can also be improved by applying an external voltage. Fig. 4(b)-(d) shows the responsivity, $PDCR$, and EQE with various bias voltages. It is seen that the FOMs are improved with a greater applied voltage due to enhanced carrier transport. At an external voltage of 5 V and a light intensity of

TABLE 1. Comparison of self-powered performance for Ga2O3 heterojunction photodetectors.

PD	*PDCR*	*R* (mA/W)	D^* (Jones)	Rise Time (ms)	Decay Time (ms)	Ref.
$CuCrO_2/Ga_2O_3$	3.5×10^4	0.1	4.7×10^{11}	350/1850	60	[34]
Diamond/β-Ga_2O_3	37.0	0.2	7.0×10^9	N/A	N/A	[35]
ZnO/β-Ga_2O_3	1.0×10^4	9.7	6.3×10^{12}	0.1	0.9	[36]
CuI/β-Ga_2O_3	4.0×10^3	8.5	6.3×10^{12}	97.8	28.9	[37]
NiO/Ga_2O_3	1.0×10^2	0.3	1.8×10^8	12/41	8/75	[38]
MoS_2/β-Ga_2O_3	1.3×10^4	2.1	1.2×10^{11}	N/A	N/A	[39]
AlN/β-Ga_2O_3	8.6×10^5	0.4	3.4×10^{12}	129	136	this work

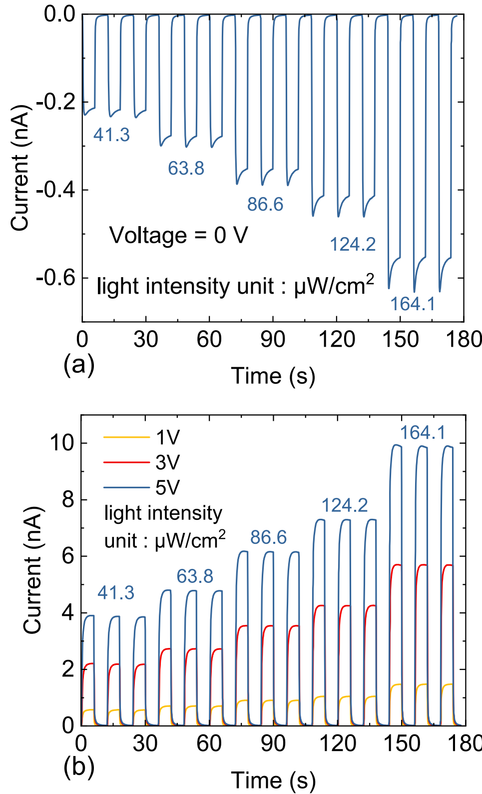

FIGURE 5. Temporal response of the β-Ga_2O_3/AlN photodetector with various light intensities at (a) 0 V and (b) 1, 3, 5 V.

41.3 μW/cm^2, the photodetector exhibits *R*, *PDCR*, and *EQE* of 4.5 mA/W, 1.5×10^4, and 2.2%, respectively, suggesting that the performance can be further improved at the expense of power consumption. In addition, the degradation caused by the improved light intensity is much lower than that of 0 V. This is because the carriers are drained rapidly by the enhanced electric field and thus fewer carriers would be recombined.

Furthermore, the temporal response of the β-Ga_2O_3/AlN photodetector is studied to determine its transient characteristics, as shown in Fig. 5. During the measurement, a duty time of 12 s and a duty cycle of 50% were used. Fig. 5(a) presents the *I-t* characteristics without applied voltage and Fig. 5(b) is that with applied voltage. It is observed that the dark current is negative, and its magnitude is enhanced with greater light intensity, as shown in Fig. 5(a). For applied voltages of 1, 3, and 5 V, positive photocurrent can be observed and the same trend can be found when the light intensity increases. Meanwhile, for self-powered operation, a visible photocurrent surge was observed at the beginning of the DUV illumination stage. With an enhanced light intensity, the surge peak was also enhanced yet vanished when an externally applied voltage was introduced.

This phenomenon can be attributed to the carrier generation/recombination relaxation process. At the start of DUV illumination, carriers are generated within the β-Ga_2O_3/AlN heterojunction and are driven to form the photocurrent at 0 V bias. Compared to a positive-voltage situation, the built-in electric field is relatively low. The insufficient built-in electric field results in the low-efficiency carrier transport and more photo-generated carriers will be recombined rather than transported. This relaxation process is the main reason for the photocurrent spike in Fig. 5(a). Providing sufficient time, the recombination/generation reaches a stable state and thus a steady photocurrent is obtained.

Another fact is that an enhanced current peak was observed when the light intensity was increased. It is ready to conclude that QFLs are much separated and the recombination process is improved in that case, leading to a more significant photocurrent overshoot. Once the external electric field was applied, the carrier transport was promoted and fewer carriers would be recombined. Therefore, the relaxation duration is almost eliminated and no significant photocurrent peak can be observed, as shown in Fig. 5(b).

In a MSM photodetector, the current peak is hardly observed since a bias voltage is applied. With a heterojunction photodetector, to pursue a self-powered operation, the device is designed to operate under a zero-bias condition. Therefore, to obtain a surge-free transient characteristic, a band alignment that features a larger built-in potential and a higher electric field is preferred. This means that the optimization of material selection and doping concentration could be beneficial.

We then further examine the transient characteristics of the heterojunction photodetector, as shown in Fig. 6(a)-(e). The response time can be extracted by $I = I_0 + Ae^{\frac{-t}{\tau}}$ [27], where I_0 is the stable state I_{photo}, A is a constant, t is the time, and τ is a time constant. The rise and decay time (τ_r and τ_d) of the β-Ga_2O_3/AlN sensor without external voltage are also displayed in Fig. 6(a)-(e). The rise time and the decay time at 41.3 μW/cm^2 are 207 ms and 159 ms, respectively. Both the rise time and the decay time are decreased with enhanced light intensity.

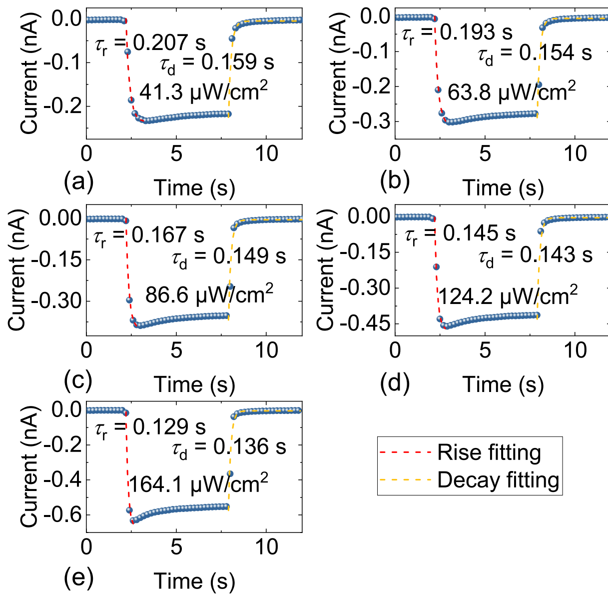

FIGURE 6. (a)-(e) Single on/off cycle of the β-Ga_2O_3/AlN heterojunction photodetector under different light intensities. The rise time and decay time are extracted and plotted in each figure.

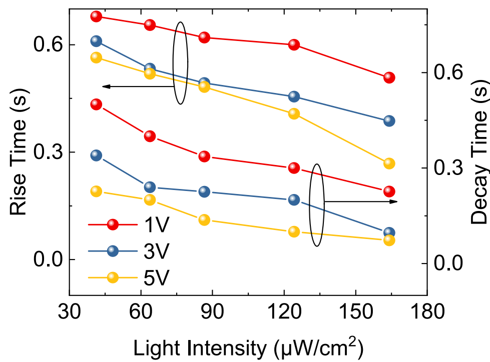

FIGURE 7. Extracted rise time and decay time of the photodetector as a function of the light intensity with applied voltages.

The response time, especially for the decay time, is strongly correlated to the SRH recombination rate. In other words, a higher recombination rate will result in a faster response time. As we mentioned above, a wider separation of the QFLs is formed when the light intensity increases. The origin of the θ<1 and the decreased response time are essentially the same, that is, more available recombination centers and improved recombination rate. Fig. 7 also shows the response time as a function of the light intensity with applied voltages. The same trend that both rise time and decay time are decreased with a higher light intensity can be found.

Although the recombination centers are beneficial to the response time, one should further improve the material quality and reduce the defects since they are unintentionally introduced and are harmful to the detection linearity. As the maturity of β-Ga_2O_3/AlN crystal growth and heteroepitaxy is under rapid development, Ga_2O_3-based heterojunction with a greater sensing performance will be realized in the near future.

IV. CONCLUSION

To conclude, in this work, we propose a β-Ga_2O_3/AlN heterojunction photodetector, and its operating principles are investigated. The *I-V* and *I-t* characteristics are measured, and the detection performance, including a photo-to-dark current ratio of 8.6×10^5, a responsivity of 0.41 mA/W, a specific detectivity of 3.4×10^{12} Jones, and an external quantum efficiency of 0.2% were achieved under 0 V bias. More importantly, by exploring the synergetic effect between the carrier transport and recombination process, this work demonstrates the Fermi-level splitting and its impact on the detection figure-of-merits. In all, this work shows a high-performance self-powered DUV photodetection and lays the foundation for further development of fully UWB photodetectors.

REFERENCES

[1] Y. Peng et al., "Arrays of solar-blind ultraviolet photodetector based on β-Ga_2O_3 epitaxial thin films," *IEEE Photon. Technol. Lett.*, vol. 30, no. 11, pp. 993–996, Jun. 2018, doi: 10.1109/LPT.2018.2826560.
[2] W. Zheng, R. Lin, J. Ran, Z. Zhang, X. Ji, and F. Huang, "Vacuum-ultraviolet photovoltaic detector," *ACS Nano*, vol. 12, no. 1, pp. 425–431, Jan. 2018, doi: 10.1021/acsnano.7b06633.
[3] M. Zhang et al., "β-Ga_2O_3-based power devices: A concise review," *Crystals*, vol. 12, no. 3, p. 406, Mar. 2022, doi: 10.3390/cryst12030406.
[4] M. Sajjad, W. M. Jadwisienczak, and P. Feng, "Nanoscale structure study of boron nitride nanosheets and development of a deep-UV photo-detector," *Nanoscale*, vol. 6, no. 9, pp. 4577–4582, Apr. 2014, doi: 10.1039/C3NR05817D.
[5] A. S. Pratiyush et al., "High responsivity in molecular beam epitaxy grown β-Ga_2O_3 metal semiconductor metal solar blind deep-UV photodetector," *Appl. Phys. Lett.*, vol. 110, no. 22, 2017, Art. no. 221107, doi: 10.1063/1.4984904.
[6] X. H. Chen et al., "High signal/noise ratio and high-speed deep UV detector on β-Ga_2O_3 thin film composed of both (400) and (201) orientation β-Ga_2O_3 deposited by the PLD method," *J. Alloys Compd.*, vol. 747, pp. 869–878, May 2018, doi: 10.1016/j.jallcom.2018.03.094.
[7] J. Yu et al., "Surface modification of β-Ga_2O_3 layer using pt nanoparticles for improved deep UV photodetector performance," *J. Alloys Compd.*, vol. 872, Aug. 2021, Art. no. 159508, doi: 10.1016/j.jallcom.2021.159508.
[8] S. Imura, K. Kikuchi, K. Miyakawa, H. Ohtake, and M. Kubota, "Low-voltage-operation avalanche photodiode based on n-gallium oxide/p-crystalline selenium heterojunction," *Appl. Phys. Lett.*, vol. 104, no. 24, 2014, Art. no. 242101, doi: 10.1063/1.4883649.
[9] S. Imura et al., "High-sensitivity image sensors overlaid with thin-film gallium oxide/crystalline selenium heterojunction photodiodes," *IEEE Trans. Electron Devices*, vol. 63, no. 1, pp. 86–91, Jan. 2016, doi: 10.1109/TED.2015.2441774.
[10] X. Chen, F. Ren, S. Gu, and J. Ye, "Review of gallium-oxide-based solar-blind ultraviolet photodetectors," *Photon. Res.*, vol. 7, no. 4, pp. 381–415, Apr. 2019, doi: 10.1364/PRJ.7.000381.
[11] Y. Qin et al., "Review of deep ultraviolet photodetector based on gallium oxide," *Chin. Phys. B*, vol. 28, no. 1, 2019, Art. no. 018501, doi: 10.1088/1674-1056/28/1/018501.
[12] D. Zhang, Z. Du, M. Ma, W. Zheng, S. Liu, and F. Huang, "Enhanced performance of solar-blind ultraviolet photodetector based on Mg-doped amorphous gallium oxide film," *Vacuum*, vol. 159, pp. 204–208, Jan. 2019, doi: 10.1016/j.vacuum.2018.10.025.
[13] P. R. Jubu and F. K. Yam, "Development and characterization of MSM UV photodetector based on gallium oxide nanostructures," *Sens. Actuators A, Phys.*, vol. 312, Sep. 2020, Art. no. 112141, doi: 10.1016/j.sna.2020.112141.

[14] P. Mukhopadhyay and W. V. Schoenfeld, "High responsivity tin gallium oxide Schottky ultraviolet photodetectors," *J. Vacuum Sci. Technol. A*, vol. 38, no. 1, 2020, Art. no. 013403, doi: 10.1116/1.5128911.

[15] S. Wang et al., "Highly-rectifying graphene/GaN Schottky contact for self-powered UV photodetector," *IEEE Photon. Technol. Lett.*, vol. 33, no. 4, pp. 213–216, Jan. 2021, doi: 10.1109/LPT.2021.3052171.

[16] Y. Wang et al., "Ultrahigh gain solar blind avalanche photodetector using an amorphous Ga_2O_3-based heterojunction," *ACS Nano*, vol. 15, no. 10, pp. 16654–16663, 2021, doi: 10.1021/acsnano.1c06567.

[17] M. Zhang et al., "High-temperature reliability of all-oxide self-powered deep UV photodetector based on ε-Ga_2O_3/ZnO heterojunction," *J. Phys. D, Appl. Phys.*, vol. 55, no. 37, 2022, Art. no. 375106, doi: 10.1088/1361-6463/ac7d1c.

[18] W. E. Mahmoud, "Solar blind avalanche photodetector based on the cation exchange growth of β-Ga_2O_3/SnO_2 bilayer heterostructure thin film," *Solar Energy Mater. Solar Cells*, vol. 152, pp. 65–72, Aug. 2016, doi: 10.1016/j.solmat.2016.03.015.

[19] S. Nakagomi, T. Sato, Y. Takahashi, and Y. Kokubun, "Deep ultraviolet photodiodes based on the β-Ga_2O_3/GaN heterojunction," *Sens. Actuators A, Phys.*, vol. 232, pp. 208–213, Aug. 2015, doi: 10.1016/j.sna.2015.06.011.

[20] J. Yu et al., "Self-powered photodetectors based on β-Ga_2O_3/4H–SiC heterojunction with ultrahigh current on/off ratio and fast response," *J. Alloys Compd.*, vol. 821, Apr. 2020, Art. no. 153532, doi: 10.1016/j.jallcom.2019.153532.

[21] Y. Hao, X. Wang, and Y. An, "A Ga_2O_3/AlN heterojunction for self-powered solar-blind photodetection with high photo-to-dark current ratio and fast response speed," *Phys. Scr.*, vol. 96, no. 12, Dec. 2021, Art. no. 125835, doi: 10.1088/1402-4896/ac2d8a.

[22] Z. Xu et al., "Zero-biased solar-blind photodetectors based on AlN/β-Ga_2O_3 heterojunctions," *Semicond. Sci. Technol.*, vol. 36, no. 6, Jun. 2021, Art. no. 065007, doi: 10.1088/1361-6641/abf3aa.

[23] M. Higashiwaki and S. Fujita, *Gallium Oxide: Materials Properties, Crystal Growth, and Devices* (Springer Series in Materials Science), vol. 293, Cham, Switzerland: Springer, 2020, doi: 10.1007/978-3-030-37153-1.

[24] A. Mondal, M. K. Yadav, S. Shringi, and A. Bag, "Extremely low dark current and detection range extension of Ga_2O_3 UV photodetector using Sn alloyed nanostructures," *Nanotechnology*, vol. 31, no. 29, Apr. 2020, Art. no. 294002, doi: 10.1088/1361-6528/ab82d4.

[25] B. Sun et al., "High-sensitive, self-powered deep UV photodetector based on p-CuSCN/n-Ga_2O_3 thin film heterojunction," *Opt. Commun.*, vol. 504, Feb. 2022, Art. no. 127483, doi: 10.1016/j.optcom.2021.127483.

[26] S. Oh, C.-K. Kim, and J. Kim, "High responsivity β-Ga_2O_3 metal–semiconductor–metal solar-blind photodetectors with ultraviolet transparent graphene electrodes," *ACS Photon.*, vol. 5, no. 3, pp. 1123–1128, Mar. 2018, doi: 10.1021/acsphotonics.7b01486.

[27] M. Zhang et al., "Study of nonthermal-equilibrium carrier recombination and transport in β-Ga_2O_3 metal–semiconductor–metal deep-ultraviolet photodetectors," *IEEE Trans. Electron Devices*, vol. 70, no. 5, pp. 2336–2341, May 2023, doi: 10.1109/TED.2023.3253671.

[28] A. Rose, "Recombination processes in insulators and semiconductors," *Phys. Rev.*, vol. 97, no. 2, p. 322, 1955.

[29] D. Zhang, W. Zheng, R. Lin, Y. Li, and F. Huang, "Ultrahigh EQE (15%) solar-blind UV photovoltaic detector with organic–inorganic heterojunction via dual built-in fields enhanced photogenerated carrier separation efficiency mechanism," *Adv Funct. Mater.*, vol. 29, no. 26, Jun. 2019, Art. no. 1900935, doi: 10.1002/adfm.201900935.

[30] R. A. Street, M. Schoendorf, A. Roy, and J. H. Lee, "Interface state recombination in organic solar cells," *Phys. Rev. B, Condens. Matter*, vol. 81, no. 20, May 2010, Art. no. 205307, doi: 10.1103/PhysRevB.81.205307.

[31] Y. Irokawa et al., "MgO/p-GaN enhancement mode metal-oxide semiconductor field-effect transistors," *Appl. Phys. Lett.*, vol. 84, no. 15, pp. 2919–2921, Apr. 2004, doi: 10.1063/1.1704876.

[32] T. L. Chu, S. S. Chu, G. Chen, J. Britt, C. Ferekides, and C. Q. Wu, "Zinc selenide films and heterojunctions," *J. Appl. Phys.*, vol. 71, no. 8, pp. 3865–3869, Apr. 1992, doi: 10.1063/1.350851.

[33] Z. Bai, J. Liu, F. Liu, and Y. Zhang, "Enhanced photoresponse performance of self-powered UV–visible photodetectors based on ZnO/Cu_2O/electrolyte heterojunctions via graphene incorporation," *J. Alloys Compd.*, vol. 726, pp. 803–809, Dec. 2017, doi: 10.1016/j.jallcom.2017.08.035.

[34] R. Zhuo et al., "A self-powered solar-blind photodetector based on a MoS_2/β-Ga_2O_3 heterojunction," *J. Mater. Chem. C*, vol. 6, no. 41, pp. 10982–10986, 2018, doi: 10.1039/C8TC04258F.

[35] B. Zhao et al., "An ultrahigh responsivity (9.7 mA W^{-1}) self-powered solar-blind photodetector based on individual ZnO–Ga_2O_3 heterostructures," *Adv Funct. Mater.*, vol. 27, no. 17, May 2017, Art. no. 1700264, doi: 10.1002/adfm.201700264.

[36] J. Yu et al., "Improved photoresponse performance of self-powered β-Ga_2O_3/NiO heterojunction UV photodetector by surface plasmonic effect of Pt nanoparticles," *IEEE Trans. Electron Devices*, vol. 67, no. 8, pp. 3199–3204, Aug. 2020, doi: 10.1109/TED.2020.2999027.

[37] C. Wu et al., "High sensitive and stable self-powered solar-blind photodetector based on solution-processed all inorganic $CuMO_2$/Ga_2O_3 pn heterojunction," *Mater. Today Phys.*, vol. 17, Mar. 2021, Art. no. 100335, doi: 10.1016/j.mtphys.2020.100335.

[38] S. Li et al., "Broadband ultraviolet self-powered photodetector constructed on exfoliated β-Ga_2O_3/CuI core–shell microwire heterojunction with superior reliability," *J. Phys. Chem. Lett.*, vol. 12, no. 1, pp. 447–453, Jan. 2021, doi: 10.1021/acs.jpclett.0c03382.

[39] Y.-C. Chen et al., "Self-powered diamond/β-Ga_2O_3 photodetectors for solar-blind imaging," *J. Mater. Chem. C*, vol. 6, no. 21, pp. 5727–5732, 2018, doi: 10.1039/C8TC01122B.